

# We are IntechOpen, the world's leading publisher of Open Access books Built by scientists, for scientists

6,900

Open access books available

186,000

International authors and editors

200M

Downloads

Our authors are among the

154

Countries delivered to

TOP 1%

most cited scientists

12.2%

Contributors from top 500 universities



WEB OF SCIENCE™

Selection of our books indexed in the Book Citation Index  
in Web of Science™ Core Collection (BKCI)

Interested in publishing with us?  
Contact [book.department@intechopen.com](mailto:book.department@intechopen.com)

Numbers displayed above are based on latest data collected.  
For more information visit [www.intechopen.com](http://www.intechopen.com)



---

# Advanced Exergy Analysis of an Integrated SOFC-Adsorption Refrigeration Power System

---

Victor Hugo Rangel-Hernández,  
Andrés M. Niño-Avenidaño,  
José J. Ramírez-Minguela,  
Juan M. Belman-Flores and  
Francisco Elizalde-Blancas

Additional information is available at the end of the chapter

<http://dx.doi.org/10.5772/intechopen.74201>

---

## Abstract

In this chapter, an exergy analysis applied to a solid oxide fuel cell (SOFC)/vapor adsorption refrigeration (VAR) system is presented. The influences of four significant parameters (current density, inlet fuel temperature, fuel utilization and steam-to-carbon ratio) on the exergy efficiency of both the SOFC stack and the SOFC-VAR system are investigated. In order to do so, a mathematical model is constructed in Engineering Equation Solver (EES) software to generate the simulations. The analysis shows that the calculated exergy efficiency is around 8% lower than the energy efficiency for both cases. Moreover, it is found that most of the causes of irreversibilities in the system are due to electronic and ionic conduction in the components. It is also shown that the exergy efficiency is substantially sensitive to fuel inlet temperature, which is evidenced by a bending-over behavior. Finally, in accordance with the calculated efficiency defects, the main exergy destructions are present in the heat exchangers, the SOFC, the afterburner and the generator.

**Keywords:** SOFC, adsorption, exergy, efficiency defect, current density

---

## 1. Introduction

Recent research developments on alternatives to generate electricity are being directed to leading-edge technologies such as solid oxide fuel cells (SOFC). A fuel cell is considered as a highly efficient, environmentally friendly device to generate affordable energy [1, 2]. It is

---

well-known that a solid oxide fuel cell converts the chemical energy of a fuel into electrical energy by means of an electrochemical reaction at high operating temperatures (600–1000°C). It is this type of reaction which makes it a more efficient way to produce electricity than a conventional steam engine that depends on a quite irreversible combustion reaction. Hence solid oxide fuel cells are attracting considerable attention from worldwide researchers.

At present, most of the studies are focusing on the development of multiproduct power generation systems to enhance significantly the overall efficiency of the system [3–7]. Furthermore, developments of hybrid systems are being expanded to run other power generation systems as trigeneration systems [8, 9], steam turbines [10, 11] and gasification [12]. In this context, a comparative energy and exergy analysis of an SOFC/GT waste heat to power conversion employing Kalina and Organic Rankine cycles is reported [13]. The study reports an exergy efficiency of 62.35% for the combined SOFC/GT-ORC system and 59.53% for the combined SOFC/GT-KC system. In another study, a new solar-based multi-generation system integrated with ammonia fuel cell and solid oxide fuel-cell-gas turbine combined cycle reports an energy and exergy efficiency increase of up to 19.3 and 17.8%, respectively, in comparison to single generation systems [14]. It is also an interesting study performed to determine the effect that the anode and cathode SOFC-stack recycling gas has on both the thermodynamic and thermo-economic performance of a proposed cooling, heating and power (CCHP) system. Therein, the results show that the total energy efficiency of the trigeneration system with anode gas recycle (Tri-SOFC-AR) is 6% larger than that of a simple case [15].

Furthermore, the energy and exergy analysis is also applied to hybrid combined cooling, heating and power (CCHP) plant coupled with a molten carbonate fuel cell (MCFC) and Stirling engine [16]. In this system, the modeling and simulation show overall energy and electrical efficiencies of 71.7 and 42.28%, respectively. Micro combined power systems are also drawing particular attention from researchers. For example, a study of a micro combined cooling heating and power (CCHP) system based on high-temperature proton exchange fuel cell (PEMFC) reports an overall efficiency of 47% under winter and normal operating conditions [17].

Some researchers are also making many studies concerning the use of alcohol fuels in SOFC integrated systems. Alcohol fuels such as methanol and ethanol are being considered as promising alternative fuels since they are fluid and some of their chemical and physical properties are similar to gasoline [3, 18]. Tippawan et al. [19] investigated the influence of changing the current density, SOFC temperature, fuel utilization and SOFC anode recirculation on the efficiency of heating cogeneration, cooling cogeneration and trigeneration for an ethanol-fueled integrated SOFC system. Therein, the trigeneration exergy efficiency increased 32% in comparison to conventional power cycles.

On the other hand, other investigations are focusing particularly on the optimization of integrated SOFC systems. Hosseinpour et al. [20] performed an exergy optimization of a cogeneration system based on a methane-fed solid oxide fuel cell (SOFC) integrated with a Stirling engine. Therein, the objective function is the exergy efficiency. In accordance with the study, the optimum value for the exergy efficiency is 56.44%. In a more complex study, a multi-objective optimization of a SOFC-GT power plant is performed [21]. In this particular case,

the cost function value and the exergy efficiency are the objective functions. Through application of a fuzzy multi-objective method, the optimum point for the cost function value is 0.043 (US\$/s) and for the exergy efficiency is 57.7%, approximately.

In this context, the present work aims to contribute to the analysis of possible affordable hybrid systems, so an exergy analysis of a solid oxide fuel cell/vapor adsorption refrigeration system is presented herein. The objective of this chapter is to investigate the influences of four significant parameters (current density, inlet fuel temperature, fuel utilization and steam-to-carbon ratio) on the exergy efficiency of both the SOFC stack and the SOFC-VAR system. In order to do so, a detailed model is constructed with the fundamental equations that govern the operation of the components. Special attention is paid to the components where most of the input exergy is destroyed. It is important to comment that the simulation is performed using engineering equation solver software. Furthermore, both SOFC and VARS models are based on reliable data and parameters obtained from a literature review. So models are calibrated and validated comparing results with data reported by, respectively, Tao et al. [22] and Herold et al. [23]. The simulation model provides mass, energy and exergy balances for each component of the system and calculates efficiency parameters such as the energy and exergy efficiency as well as the efficiency defects.

## 2. Energy system description

The schematic flow diagram of the integrated SOFC-Adsorption system considered herein is depicted in **Figure 1**. The energy system consists of an SOFC stack with internal reforming of feed gas at the anode side, an afterburner, a mixer, three pre-heaters and a DC/AC inverter. Anode and cathode exit streams are fed into the afterburner, the exhaust gas is then used to preheat the supply of fuel and air. The high-grade heat yielded in the SOFC reaction is used to perform the reforming process. In order to improve the overall efficiency of the SOFC, the exhaust gas from the stack enters a LiBr-H<sub>2</sub>O-based vapor adsorption refrigeration system (VARS) coupled to it. **Table 1** presents the physical characteristics of an intermediate temperature, anode-supported planar SOFC as reported in [24].

For the sake of simplicity, several assumptions have been considered in the present analysis. The study is carried out under thermodynamic equilibrium and steady-state conditions (**Table 2**). Kinetic and potential energy effects are negligible. The assumptions are:

- A. For the solid oxide fuel cell:
  1. Air consists of 79% N<sub>2</sub> and 21% O<sub>2</sub>.
  2. All gases are considered as ideal gases.
  3. Gas mixture at the fuel channel exit is at chemical equilibrium.
  4. Fuel cell is completely insulated, so there is no heat interaction with the environment.
  5. Contact resistances are negligible.



3. Water is considered as saturated vapor at state j.
4. Pressure in generator and condenser are equivalent.
5. Pressure in the evaporator and absorber are equivalent.

Anode exchange current density ( $i_{oa}$ )	0.65 A/cm <sup>2</sup>
Cathode exchange current density ( $i_{oc}$ )	0.25 A/cm <sup>2</sup>
Effective gaseous diffusivity through the anode ( $D_{a,eff}$ )	0.2 cm <sup>2</sup> /s
Effective gaseous diffusivity through cathode ( $D_{c,eff}$ )	0.05 cm <sup>2</sup> /s
Anode thickness ( $L_a$ )	500 $\mu$ m
Cathode thickness ( $L_c$ )	50 $\mu$ m
Electrolyte thickness ( $L_e$ )	10 $\mu$ m
Number of cells	11,000
Active surface area	0.01 m <sup>2</sup>

**Table 1.** Characteristics of the SOFC as reported in [24].

<b>Input data</b>	
Temperature difference between SOFC inlet and outlet	100 K
Fuel cell inlet temperature	1000 K
Fuel utilization factor	85%
Steam-to-carbon ratio	2.5
Fuel cell pressure drop	2%
Heat exchangers pressure drop	3%
Afterburner pressure drop	5%

**Table 2.** Operating conditions of the SOFC stack.

### 3. SOFC mathematical modeling

#### 3.1. Electrochemical model

Modeling of the electrochemical part can be as complicate as the study requires it, and most of the current literature provides basic models developed under the zero-dimensional assumption [6, 8, 25]. The main idea of such modeling is to have mathematical equations that mimic the connection between the chemical energy of the fuel and the electrical power. So, the mechanisms of reaction involved are:

For the steam reforming reaction:



For the shifting reaction:



Thus the net electrochemical reaction of the fuel cell is given as:



Reforming and shifting reactions are carried out within the fuel cell stack, so the energy required for the reaction is directly supplied by the fuel cell as heat. The real velocity at which both chemical and electrochemical reactions are carried out are based on the following equilibrium reactions:

For the real reforming reaction:



For the real shifting reaction:



For the real net electrochemical reaction:



where  $X_r$ ,  $Y_r$  and  $Z_r$  represent the conversion ratios during the reactions.

The equilibrium constants for the reforming and shifting reactions can be formulated as a function of the operating temperature as follows:

$$\text{Log}_{10}K_{r,s} = A_{r,s}T^4 + B_{r,s}T^3 + C_{r,s}T^2 + D_{r,s}T + E_{r,s} \quad (7)$$

The values of the constants are given in **Table 3** as suggested in [26].

	Reforming	Shifting
A	$-2.63121 \times 10^{-11}$	$5.47301 \times 10^{-12}$
B	$1.24065 \times 10^{-7}$	$-2.57479 \times 10^{-8}$
C	$-2.25322 \times 10^{-4}$	$4.63742 \times 10^{-5}$
D	$1.95028 \times 10^{-1}$	$-3.91500 \times 10^{-2}$
E	-66.1396	13.2097

**Table 3.** Constant values for the equilibrium constant equation.

The equilibrium constants can also be determined as a function of the molar fraction of each species as now described.

For the reforming reaction:

$$\ln(K_r) = \frac{(y_{CO_{11}}^{CO})(y_{H_2_{11}}^{H_2})^3}{(y_{H_2O_{11}}^{H_2O})(y_{CH_4_{11}}^{CH_4})} * \left[ \frac{P}{P_0} \right]^2 \quad (8)$$

For the shifting reaction:

$$\ln(K_s) = \frac{(y_{H_2_{11}}^{H_2})(y_{CO_2_{11}}^{CO_2})}{(y_{CO_{11}}^{CO})(y_{H_2O_{11}}^{H_2O})} \quad (9)$$

Here, each equilibrium molar fraction of species  $i$  is represented by  $y_{eq}^i$  and it can be written as a ratio between the equilibrium number of moles of species  $i$  and the total number of moles at equilibrium.

$$y_{eq}^i = \frac{\dot{n}_{eq}^i}{\dot{n}_{eq}} \quad (10)$$

On the other hand, the equations used in the modeling for calculating the maximum voltage achievable by the solid oxide fuel cell are:

$$V_{SOFC} = V_N - V_{Loss} \quad (11)$$

where  $V_N$  represent the Nerts voltage and  $V_{Loss}$  stands for the voltage losses. It is important to recall that after a SOFC delivers electrical current, its components exhibit a resistance which results in voltage losses. These voltage losses are generally classified as ohmic, activation and concentration polarization losses. Accordingly,

$$V_N = -\frac{\Delta g_{rxn}^o}{2F} + \frac{\bar{R}T_{o,SOFC}}{2F} \ln \left( \frac{a_{H_2}^{H_2} a_{O_2}^{O_2^{1/2}}}{a_{H_2O}^{H_2O}} \right) \quad (12)$$

$$V_{Loss} = \Delta V_{ohm} + \Delta V_{act} + \Delta V_{conc} \quad (13)$$

For simplicity, the total ohmic losses can be evaluated through the equation

$$\Delta V_{ohm} = i \cdot r \quad (14)$$

$$r = \delta \cdot \rho \quad (15)$$

$$\rho = \xi e^{\alpha/T} \quad (16)$$

where  $r$  is the area-specific resistance which depends on material thickness,  $\delta$ , and on the SOFC operating temperature because of the resistivity exponential dependence. For further details of the model see [1, 7, 26].

As for the concentration losses, they are worked out using the Fick's Law of diffusion and the definition of the limiting current density  $i_L$  (corresponding to a surface concentration value of zero) [27]:

$$i = \frac{nFD(C_B - C_A)}{3.6\delta} \quad (17)$$

$$i_L = \frac{nFDC_B}{3.6\delta} \quad (18)$$

hereafter

$$\Delta V_{conc} = \frac{RT}{nF} \ln \left( \frac{C_s}{C_B} \right) = \frac{RT}{nF} \ln \left( 1 - \frac{i}{i_L} \right) \quad (19)$$

Finally, the activation losses can be described by the Butler-Volmer equation [1]:

$$i = i_o \left[ \text{Exp} \left( \alpha \frac{nF}{RT} V_{act} \right) - \text{Exp} \left( -(1 - \alpha) \frac{nF}{RT} V_{act} \right) \right] \quad (20)$$

where  $i_o$  is referred to as the exchange current density. So applying Eq. (20) to both anode and cathode half reactions, it becomes

$$i_{o,anode} = \gamma_{anode} \left( \frac{P_{H_2}}{P_{ref}} \right) \left( \frac{P_{H_2O}}{P_{ref}} \right) \text{Exp} \left( -\frac{V_{act,anode}}{RT} \right) \quad (21)$$

$$i_{o,cathode} = \gamma_{cathode} \left( \frac{P_{O_2}}{P_{ref}} \right)^{0.25} \text{Exp} \left( -\frac{V_{act,cathode}}{RT} \right) \quad (22)$$

Accordingly, the activation losses can be calculated as follows

$$\Delta V_{act} = A \ln \left( \frac{i}{i_o} \right) \quad (23)$$

$$A = \frac{RT}{n\alpha F} \quad (24)$$

However, Eq. (23) is only valid as long as the current density is higher than the exchange current density, see [2, 3].

Accordingly, the current density can be worked out as:

$$j = \frac{n_e F z}{A_c} \quad (25)$$

where  $A_c$  is referred to as the cell activation area. Then, the total electrical power generated directly from the SOFC stack is given by

$$\dot{W}_{SOFC,stack} = NV_c j A_c \tag{26}$$

whereas the net electrical power results from subtracting the power consumed by other components, that is,

$$\dot{W}_{SOFC,net} = \dot{W}_{SOFC} \eta_{inv} - \dot{W}_{comp,i} \tag{27}$$

where  $\eta_{inv}$  is the inverter efficiency.

### 3.2. Thermodynamic model

In order to model the distribution of energy and exergy in the SOFC-VARS system, it is important to set both the boundary of the entire system and control volumes for each component as depicted in **Figure 1**. Both energy and exergy analyses are performed at steady-state condition. Kinetic and potential energy changes are negligible.

#### 3.2.1. General energy balance

In accordance with the first law of thermodynamics, the energy balance for any system can be written as:

$$\frac{dE_{CV}}{dt} = \sum_j \dot{Q}_j - \sum_j \dot{W}_j + \sum_i \dot{m}_i e - \sum_o \dot{m}_o e \tag{28}$$

Based on Eq. (28) and **Figure 1**, the energy balance for the SOFC and VARS system is provided, respectively, in **Tables 4** and **5**. And, **Table 6** provides the energy performance parameters to be evaluated.

Component	Energy balance	Eq.
Pump 1	$\dot{W} = \dot{m}_1(h_2 - h_1)$	(29)
Fuel compressor	$\dot{W} = \dot{m}_2(h_5 - h_4)$	(30)
Air compressor	$\dot{W} = \dot{m}_3(h_8 - 7)$	(31)
Heat exchanger 1	$\dot{m}_2 h_2 + \dot{m}_{15} h_{15} = \dot{m}_3 h_3 + \dot{m}_{16} h_{16}$	(32)
Heat exchanger 2	$\dot{m}_5 h_5 + \dot{m}_{16} h_{16} = \dot{m}_6 h_6 + \dot{m}_{17} h_{17}$	(33)
Heat exchanger 3	$\dot{m}_8 h_8 + \dot{m}_{17} h_{17} = \dot{m}_9 h_9 + \dot{m}_{18} h_{18}$	(34)
Mixing chamber	$\dot{m}_3 h_3 + \dot{m}_6 h_6 + \dot{m}_{12b} h_{12b} = \dot{m}_{11} h_{11}$	(35)
SOFC	$\dot{m}_3 h_3 + \dot{m}_6 h_6 + \dot{m}_{10} h_{10} = \dot{m}_{13} h_{13} + \dot{m}_{14} h_{14} + \dot{W}_{SOFC}$	(36)
After burner	$\dot{m}_{13} h_{13} + \dot{m}_{14} h_{14} = \dot{m}_{15} h_{15}$	(37)

**Table 4.** Energy balance for the SOFC's components.

Component	Energy balance	Eq.
Solution pump	$\dot{W}_{\text{pump}} = \dot{m}_{14}(h_b - h_a)$	(38)
Solution heat exchanger	$\dot{Q}_{HX} = \dot{m}_{15}(h_c - h_b) = \dot{m}_d(h_d - h_e)$	(39)
Steam generator	$\dot{Q}_{SG} = \dot{m}_d h_d + \dot{m}_g h_g - \dot{m}_c h_c = \dot{m}_{18}(h_{18} - h_{19})$	(40)
Solution valve	$h_e = h_f h_e = h_f$	(41)
Condenser	$\dot{Q}_{\text{Cond}} = \dot{m}_g(h_g - h_h) = \dot{m}_l(h_l - h_k)$	(42)
Refrigerant valve	$h_h = h_i$	(43)
Evaporator	$\dot{Q}_{\text{evap}} = \dot{m}_i(h_j - h_i) = \dot{m}_m(h_m - h_n)$	(44)
Absorber	$\dot{Q}_{\text{abs}} = \dot{m}_f h_f + \dot{m}_j h_j - \dot{m}_a h_a = \dot{m}_o(h_p - h_o)$	(45)

**Table 5.** Energy balance for the VARS's components.

Parameter	Definition	Eq.
SOFC stack AC electrical power	$\dot{W}_{AC} = \dot{W}_{\text{SOFC}}/\eta_{\text{inv}}$	(46)
SOFC net electrical power	$\dot{W}_{\text{net}} = \dot{W}_{AC} - \dot{W}_{P1} - \dot{W}_{P2} - \dot{W}_{C1} - \dot{W}_{C2}$ P = pump; C = compressor	(47)
Fuel cell efficiency	$\eta_{FC} = \frac{\dot{W}_{AC}}{\dot{m}_{\text{fuel}} \text{LHV}}$	(48)
SOFC stack net efficiency	$\eta_{\text{SOFC}} = \frac{\dot{W}_{\text{net}}}{\dot{m}_{\text{fuel}} \text{LHV}}$	(49)
Cogeneration efficiency	$\eta_{FC} = \frac{\dot{W}_{AC} + \dot{Q}_{\text{evap}}}{\dot{m}_{\text{fuel}} \text{LHV}}$	(50)
Coefficient of performance	$\text{COP} = \frac{\dot{Q}_{\text{evap}}}{\dot{Q}_{\text{gen}}}$	(51)

**Table 6.** General parameters of performance.

### 3.2.2. General exergy balance

Provided that the SOFC presents both chemical and electrochemical reactions, it is required to consider two exergy contributions, namely, physical and chemical exergy. Hence the general exergy balance for a given control volume is:

$$\dot{I} = \sum_j \left(1 - \frac{T_o}{T_j}\right) \dot{Q}_j - \dot{W}_{CV} + \sum_{\text{inlet}} \dot{E}x_{\text{inlet}} - \sum_{\text{outlet}} \dot{E}x_{\text{outlet}} \quad (52)$$

where  $\dot{I}$  is referred to as the exergy destruction ratio, see [28].

The physical and chemical exergy are evaluated, respectively, using the following equations [7]:

$$\dot{E}x_{ph} = \sum_i \dot{n}_i [(\bar{h}_i - \bar{h}_o) - T_o(\bar{s}_i - \bar{s}_o)] \quad (53)$$

$$\dot{E}x_{ch} = \dot{n} \left[ \sum_i y_i \bar{e}_{x,i}^{ch,o} + \bar{R}T_o \sum_i y_i \ln(y_i) \right] \quad (54)$$

where  $\bar{e}_{x,i}^{ch,0}$  is the standard chemical exergy as proposed by Szargut et al. [29];  $y_i$  refers to the molar fraction of each species.

For the particular case of the VARS subsystem, the exergy of the Li-Br solution can be calculated using the model proposed by Palacios-Berech [30]. The model calculates the chemical exergy of the dissolution as a function of the H<sub>2</sub>O and LiBr activities, the molality and the osmotic coefficient as described in **Table 7**.

where  $a_i$  and  $b_i$  are constants whose values are provided in **Table 8** [31].

The exergy balances for SOFC and VARS subsystems are given respectively in **Tables 9** and **10**.

In this work, the exergy analysis of the system is simplified using the general definition of exergy efficiency which is referred to as the ratio between the exergy rate of the product and the exergy rate of the fuel. Consequently, it is possible to write the exergy efficiency of the SOFC stack as:

$$\eta_{SOFC} = \frac{\dot{W}_{SOFC}}{\dot{E}x_{fuel}} \quad (61)$$

Parameter	Exergy analysis	Eq.
Molality in saturated state	$m_{sat} = \frac{x_{LiBr,sat}}{(1-x_{LiBr,sat})\bar{M}_{LiBr}}$	(55)
Molality at any state	$m_{sat} = \frac{x_i}{(1-x_i)\bar{M}_{LiBr}}$	(56)
H <sub>2</sub> O activity	$\ln(a_{H_2O}) = -\phi \cdot v \cdot m \cdot \bar{M}_{H_2O}$	(57)
Osmotic coefficient	$\phi = 1 + \sum_{i=1}^6 a_i \cdot m^i + \frac{p}{2v} \sum_{i=1}^2 i \cdot b_i \cdot m^{i/2}$	(58)
LiBr activity	$a_{LiBr} = -v \left[ \ln(m) + \sum_{i=1}^6 \frac{i+2}{i} \left( a_i + i \frac{b_i}{2v} \right) \cdot m^{i/2} \right] m^{m_{sat}}$	(59)
Chemical exergy	$\dot{E}_{ch} = \frac{RT_0}{M_{sol}} \left( y_{H_2O} \ln(a_{H_2O}) + y_{LiBr} \ln(a_{LiBr}) \right)$	(60)

**Table 7.** Parameters to calculate the chemical exergy of the Li-Br solution.

	j = 0	j = 1	j = 2
a <sub>1j</sub>	-2.19631551 × 10 <sup>1</sup>	4.9372316 × 10 <sup>3</sup>	-6.55484056 × 10 <sup>5</sup>
a <sub>2j</sub>	-3.810475 × 10 <sup>3</sup>	2.611535 × 10 <sup>6</sup>	-3.6699691 × 10 <sup>8</sup>
a <sub>3j</sub>	1.228085 × 10 <sup>5</sup>	-7.718792 × 10 <sup>7</sup>	1.039856 × 10 <sup>10</sup>
a <sub>4j</sub>	-1.471674 × 10 <sup>6</sup>	9.195285 × 10 <sup>8</sup>	-1.189450 × 10 <sup>11</sup>
a <sub>5j</sub>	7.765821 × 10 <sup>6</sup>	-4.937567 × 10 <sup>9</sup>	6.317555 × 10 <sup>11</sup>
a <sub>6j</sub>	-1.511892 × 10 <sup>7</sup>	9.839974 × 10 <sup>9</sup>	-1.2737 × 10 <sup>12</sup>
b <sub>1j</sub>	3.07410 × 10 <sup>-4</sup>	-1.86321 × 10 <sup>-1</sup>	2.738714 × 10 <sup>1</sup>
b <sub>2j</sub>	-4.080794 × 10 <sup>-4</sup>	2.16081 × 10 <sup>-1</sup>	-2.5175971 × 10 <sup>1</sup>

**Table 8.** Value of constants  $a_i$  and  $b_i$  as suggested in [8].

whereas the exergy efficiency of cogeneration is defined in this work as:

$$\eta_{SOFC} = \frac{\dot{W}_{net,SOFC} + \dot{E}x_{evap}^Q}{\dot{E}x_{fuel}} \quad (62)$$

Component	Exergy balance	Eq.
Pump 1	$\dot{E}_{D,P1} = \dot{W}_{P,1} + \dot{E}x_1 - \dot{E}x_2$	(55)
Fuel compressor	$\dot{E}_{D,C1} = \dot{W}_{comp1} + \dot{E}x_4 - \dot{E}x_5$	(56)
Air compressor	$\dot{E}_{D,C2} = \dot{W}_{comp2} + \dot{E}x_8 - \dot{E}x_9$	(57)
Heat exchanger 1	$\dot{E}_{D,HX1} = \dot{E}x_2 + \dot{E}x_{15} - \dot{E}x_3 - \dot{E}x_{16}$	(58)
Heat exchanger 2	$\dot{E}_{D,HX2} = \dot{E}x_5 + \dot{E}x_{16} - \dot{E}x_6 - \dot{E}x_{17}$	(59)
Heat exchanger 3	$\dot{E}_{D,HX3} = \dot{E}x_9 + \dot{E}x_{17} - \dot{E}x_{10} - \dot{E}x_{18}$	(60)
Mixing chamber	$\dot{E}_{D,MC} = \dot{E}x_3 + \dot{E}x_6 + \dot{E}x_{12b} - \dot{E}x_{11}$	(61)
SOFC stack	$\dot{E}_{D,SOFC} = \dot{E}x_{10} + \dot{E}x_{11} - \dot{E}x_{12} - \dot{E}x_{14} - \dot{W}_{SOFC}$	(62)
Afterburner	$\dot{E}_{D,AB} = \dot{E}x_{14} + \dot{E}x_{13} - \dot{E}x_{15}$	(63)

**Table 9.** Exergy balance equations for the SOFC's components.

Component	Exergy balance	Eq.
Solution pump	$\dot{E}_{D,Psol} = \dot{W}_{b,sol} + \dot{E}x_a - \dot{E}x_b$	(55)
Solution heat exchanger	$\dot{E}_{D,HXsol} = \dot{E}x_d + \dot{E}x_b - \dot{E}x_c - \dot{E}x_e$	(56)
Steam generator	$\dot{E}_{D,SG} = \dot{E}x_{18} + \dot{E}x_c - \dot{E}x_{19} - \dot{E}x_d - \dot{E}x_g$	(57)
Condenser	$\dot{E}_{D,cond} = \dot{E}x_g + \dot{E}x_k - \dot{E}x_h - \dot{E}x_l$	(58)
Evaporator	$\dot{E}_{D,evap} = \dot{E}x_i + \dot{E}x_m - \dot{E}x_j - \dot{E}x_n$	(59)
Absorber	$\dot{E}_{D,Abs} = \dot{E}x_j + \dot{E}x_f + \dot{E}x_o - \dot{E}x_a - \dot{E}x_p$	(60)

**Table 10.** Exergy balance equations for the VARS' components.

#### 4. Validation of SOFC and VARS models

Any mathematical model is not useful if this has not been previously validated with either experimental data or previous works. Hence validation of both SOFC and VARS models is carried out in this section. For the case of the SOFC model, this is validated with a previous work introduced by Tao et al. [22]. As for the VARS model, it is validated with data taken from Herold et al. [23].

From **Figure 2**, it can be deduced that the model developed here has a good fit along a broad range of current density, but shows a slight deviation at the end of the curve (at higher current densities) which can be considered to be negligible (error less than 3%). Likewise, the VARS

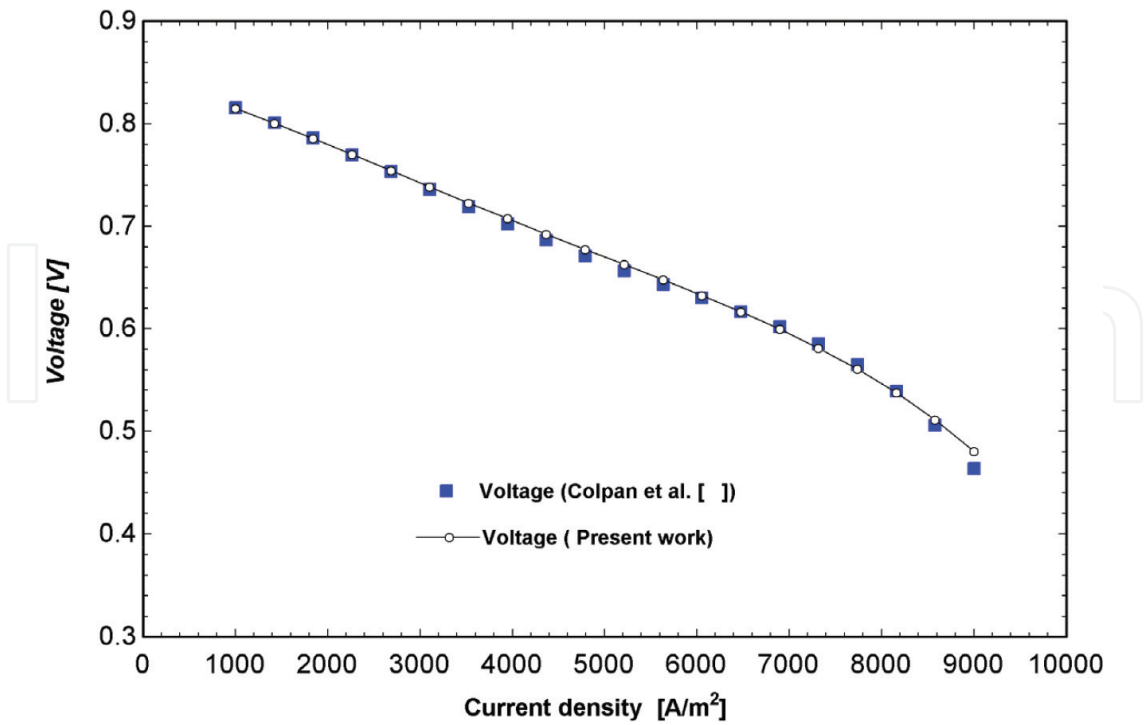


Figure 2. Characteristic polarization curve.

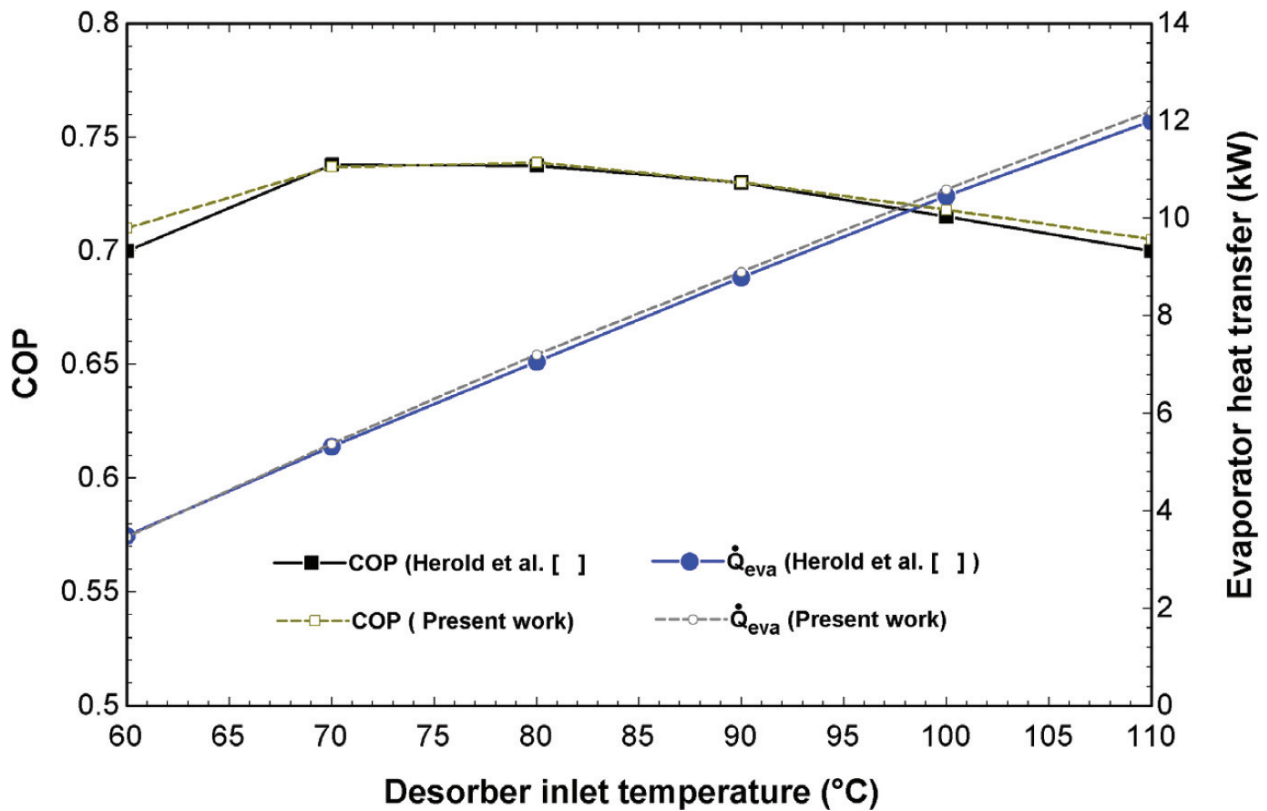


Figure 3. Characteristic curves of a vapor-adsorption refrigeration system.

model used herein is seen to exhibit good agreement with previous works, **Figure 3**. In this particular case, the validation is worked out by comparison of two important parameters used to evaluate the performance of an adsorption refrigeration system, namely, the coefficient of performance (COP) and the rate of heat transfer in the evaporator as a function of operation temperature of the generator.

## 5. Results and discussion

For the actual analysis, the current density, operation temperature, fuel utilization factor and steam-to-carbon ratio are considered as decision variables. The thermodynamic performance of the SOFC and the cogeneration system, i.e. its exergy efficiency, is then obtained by varying the decision variables over an acceptable operation range. So the variations of the exergetic efficiencies with such decision variables are explained to understand their nature.

### 5.1. Current density

One of the important parameters used to characterize the performance of a fuel cell stack is the current density when plotted versus the cell voltage, known as the polarization curve as shown in **Figure 4**. Hence it is important to study its effect on both the SOFC and the global exergy efficiencies.

The calculated variations of both energy ( $\eta$ ) and exergy ( $\psi$ ) efficiencies of the SOFC stack with current density under a constant  $U_f = 0.85$  and  $T = 1000$  K are depicted in **Figure 4**. It clearly shows the dependence of efficiency on current density.

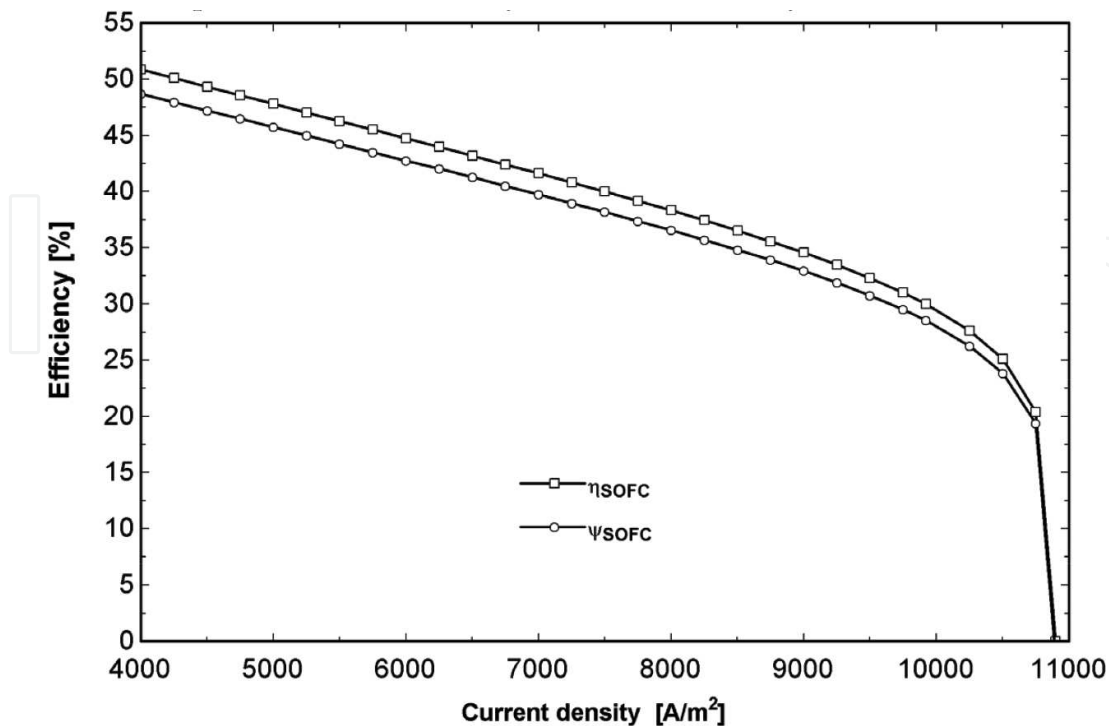


**Figure 4.** Variation of the SOFC energy and exergy efficiencies with respect to current density.

As expected, the calculated values for the exergy efficiency are slightly lower than those worked out for the energy efficiency. The reason is because the energy analysis does not take into account irreversibilities generated into the SOFC stack, so it assumes that more useful energy is available. Another important implication of **Figure 4** is that lowering current density increases both efficiencies as reported in literature [8], which is due largely to the reduction of voltage losses at lower current densities in accordance with literature [1].

The effect of current density on both efficiencies is further expanded to the whole system (cogeneration system) as evidenced in **Figure 5**. Moreover, it is observed that the first law efficiency of the cogeneration system is 15% higher than the first law efficiency of the SOFC attack alone. Likewise, the exergy efficiency maintains such a percentage difference. This is expected because the sensible heat of the stack gas is captured and converted into useful thermal energy to drive the adsorption refrigeration system. So cooling is available as second product. Furthermore, it is noteworthy to mention that the overall exergy efficiency is similar to other previous works [8, 32].

**Figure 6** shows the results of the calculated exergy efficiencies for both SOFC stack and cogeneration system as a function of the fuel utilization factor. It is very clear that lowering the operating temperature at a given  $U_F$ , the exergy efficiency increases. This applies to both the SOFC stack and the cogeneration system. For the particular case of the cogeneration system, lowering temperature from 1000 to 900 K at  $U_F = 0.85$ , the exergy efficiency increases by roughly 15%. Whereas, for the SOFC stack, its exergy efficiency increases by only 10%. This behavior stems from the fact that at lower temperatures the effect of leakage current is less significant, which causes the exergy efficiency to rise. It is, however, possible that at lower temperatures the polarization losses increase too. To some extent, it is desirable to operate at

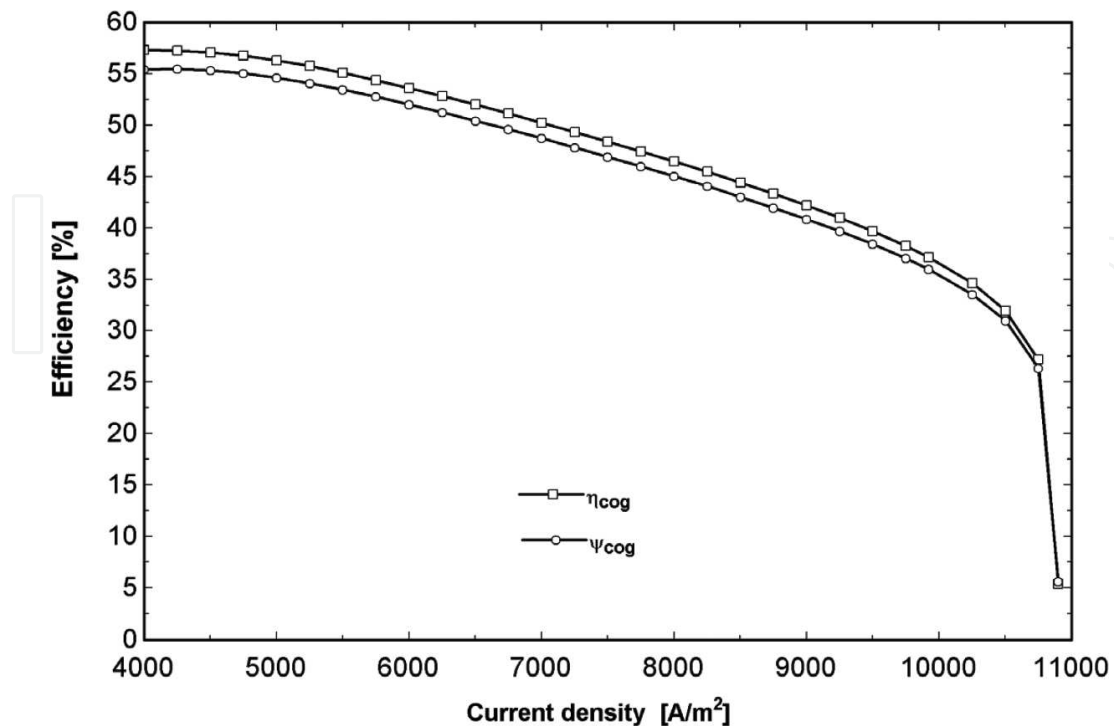


**Figure 5.** Variation of the cogeneration energy and exergy efficiencies with respect to current density.

$U_F$  values lower than 0.85 and low temperatures as efficiently as possible. Consistent with **Figure 6**, the effect of temperature on exergy efficiency can be better studied when the temperature is expanded to a wider range as depicted in **Figure 7**.

In reference to the cogeneration system, it strongly suggests that the SOFC has to operate within a range between 850 and 950 K as to boost the global exergy efficiency. A noticeable trend is that lowering  $U_F$  at a given temperature, the exergy efficiency of the SOFC increases in contrast to **Figure 6**. The reason is because in spite of increasing  $U_F$ , which is assumed to increase the useful external current, there are other types of irreversibilities caused mainly by electronic and ionic conduction throughout the SOFC components (i.e. leakage currents [1]) that determine these atypical bending-over exergy efficiency curves. For the sake of comparison, a previous work [8] reports lower exergy efficiencies, for the cogeneration system, at different inlet temperature. The reason is because of the different  $U_f$  values used in this work.

On the other hand, the steam-to-carbon ratio (SC) is one of the key parameters in the operation of a SOFC that is worth analyzing. In particular, the SC defines whether carbon deposition at cell anode is built up, which causes that more heat is generated and less  $H_2$  is consumed in the electrochemical reaction. In this respect, **Figure 8** shows that at higher SC ratios, the exergy efficiency of the SOFC stack and of the cogeneration system slightly decreases as a result of the less chemical energy converted into electrical energy as previously explained.

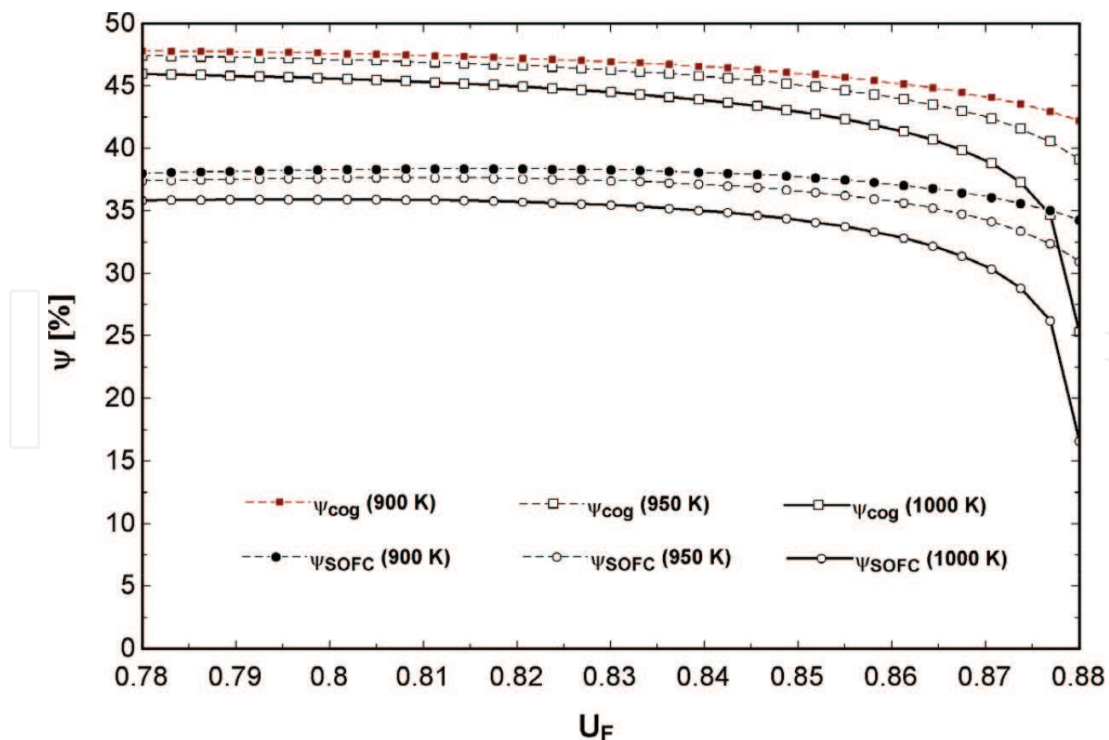


**Figure 6.** Variation of exergy efficiency with  $U_F$  at three different inlet fuel temperatures.

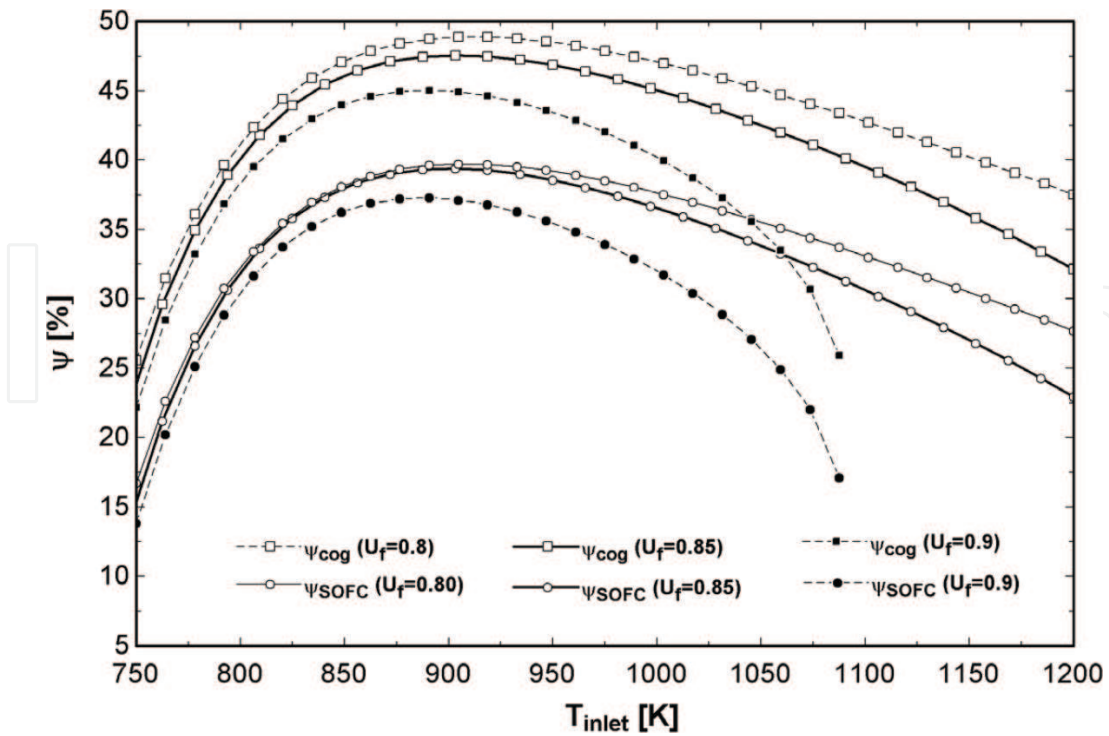


Figure 7. Variation of exergy efficiency with inlet fuel temperature at three different levels of  $U_F$ .

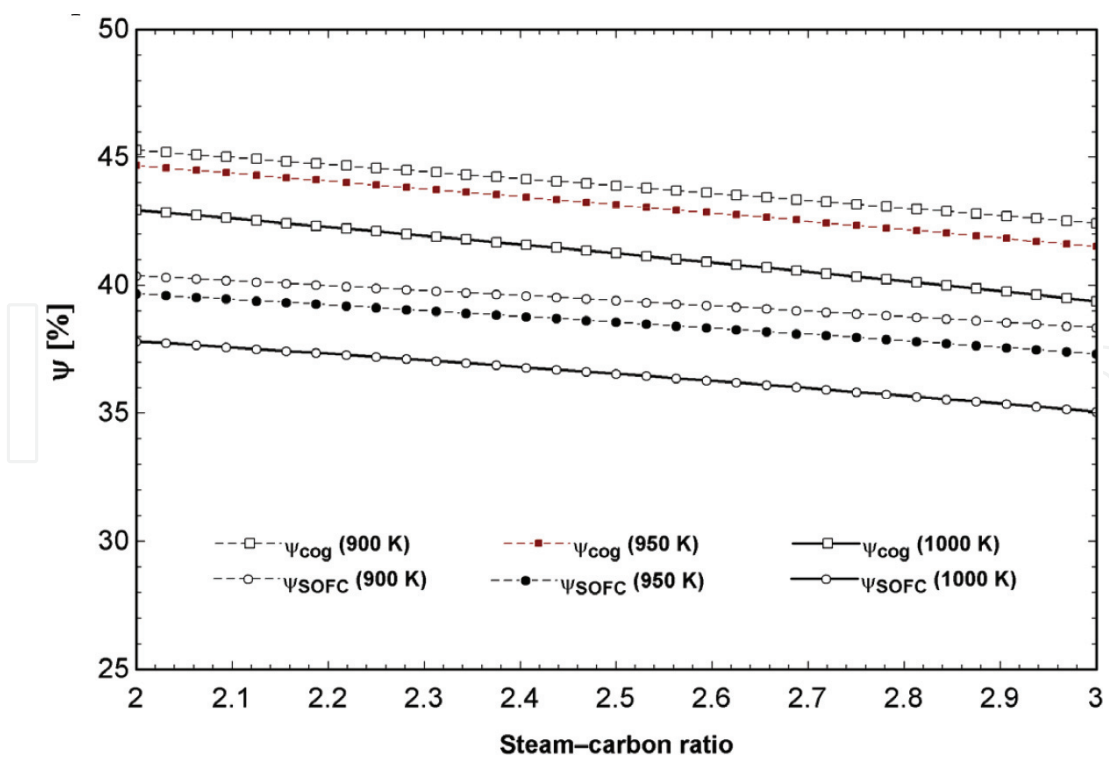
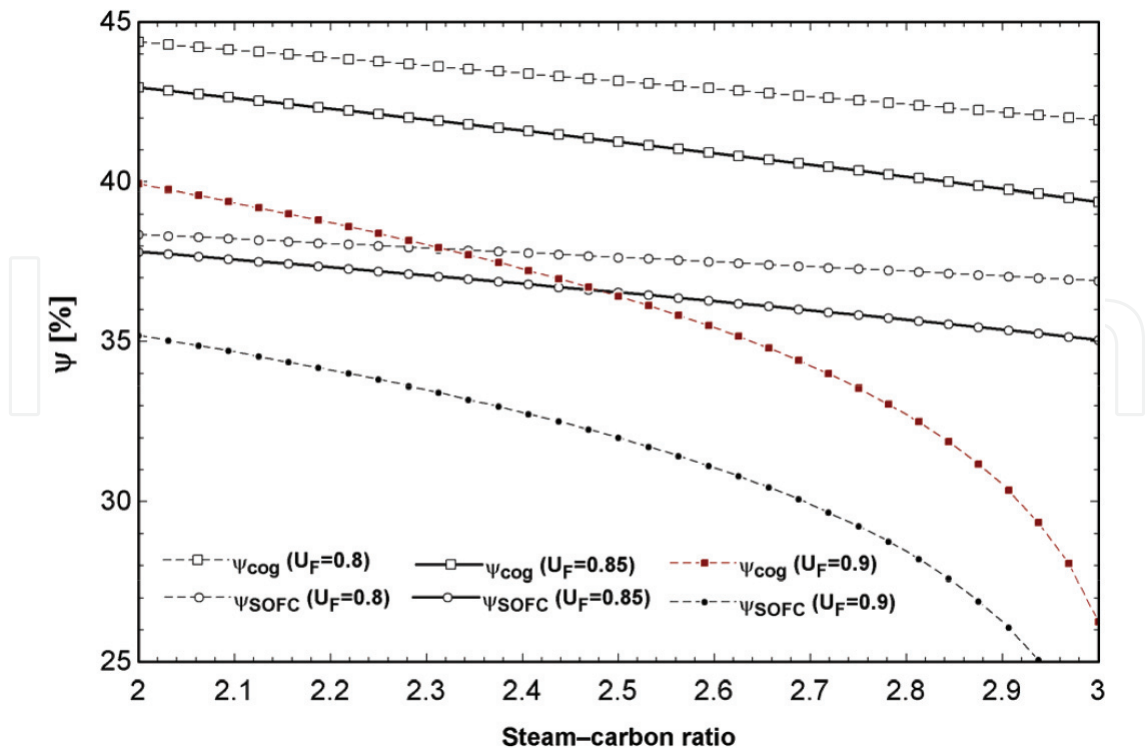


Figure 8. Effect of the steam-to-carbon ratio on exergy efficiency at three different inlet fuel temperatures.

Furthermore, a noticeable trend is that lowering temperature at a given SC ratio, both exergy efficiencies increases in agreement to **Figure 7**. In order to show the effect of  $U_F$  on exergy efficiency and at given values of SC ratio, **Figure 9** is presented. It is worth observing that exergy efficiency is slightly sensitive to SC ratio at  $U_F$  lower than 0.85. In contrast, at higher  $U_F$  values than 0.85, the effect is considerably more noticeable. It is also interesting the bending-over behavior appearing at  $U_F = 0.9$ , which is the result of other voltage losses as explained above. To be consistent, **Figure 6** shows that at higher values of  $U_F$  the exergy efficiency bends over as occurs in **Figure 7**.

Finally, **Figure 10** depicts the calculated efficiency defect,  $\delta$ , for the most representative components of the total system (i.e. SOFC-VARS system). It is worth mentioning that the efficiency defect represents the portion of exergy or useful energy that is destroyed in each component [28]. For any case, it is noticeable that the component where the most exergy is destroyed is the heat exchanger 3 (coinciding with a previous work [8]), which is located at the end of the SOFC stack, the reason is because this is the largest heat exchanger and controls the heat that is sent to the generator of the adsorption refrigeration system.

Another noticeable observation is that increasing current density the efficiency defect of the SOFC, afterburner and heat exchanger increases, respectively, 10, 30 and 35% roughly (**Figure 10**). Moreover, it is observed from this figure that the other components are not considerably affected with respect to the current density of the SOFC. This explains why the exergy efficiency is lower than the energy efficiency discussed in **Figure 4**.



**Figure 9.** Effect of the steam-to-carbon ratio on exergy efficiency at three different levels of  $U_F$  ratios.

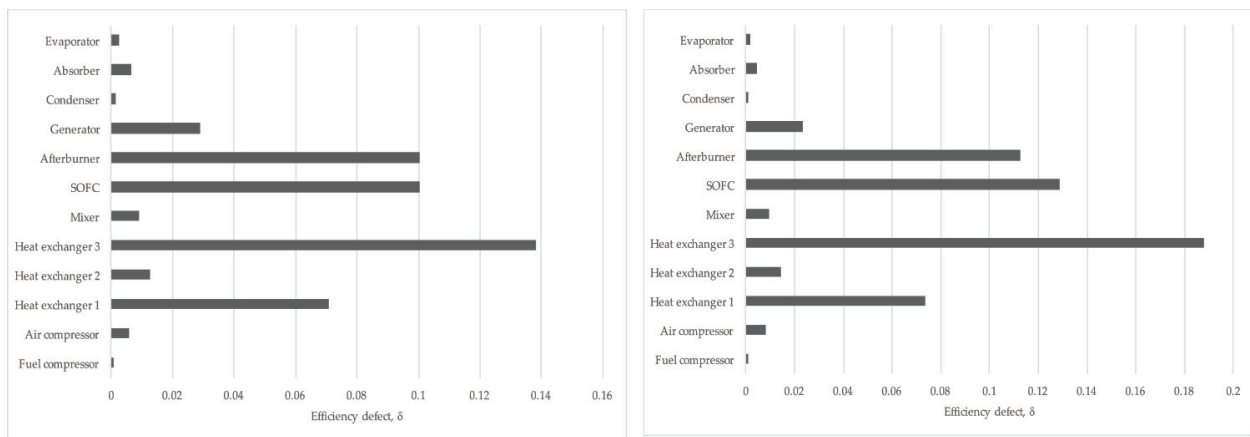


**Figure 10.** Efficiency defect,  $\delta$ , for the total system: a)  $U_F = 0.85$ ,  $T = 1000$  K and  $i = 500$  A/m<sup>2</sup>, b)  $U_F = 0.85$ ,  $T = 1000$  K and  $i = 800$  A/m<sup>2</sup>.

## 6. Conclusions

A solid oxide fuel cell/adsorption refrigeration system for electricity and cooling generation is evaluated in terms of exergy. From a thermodynamic standpoint, a combined system is a highly efficient way of making use of heat which would otherwise be lost during the production of electricity and converts it into useful thermal energy so as to boot a vapor adsorption refrigeration system as described herein. All the mathematical models are thoroughly described in order to provide a robust and thorough exergy analysis of the system. Hence the following conclusions are worked out:

1. It is interesting to mention that applying a first law analysis it is not sufficient to evaluate the amount of usable energy that is destroyed throughout the system as evidenced in **Figure 4**.
2. The first law efficiency and second law efficiency of the SOFC stack and of the cogeneration system are affected with the SOFC current density.
3. The effect of the fuel utilization factor ( $U_F$ ) on the exergy efficiency of the cogeneration and the SOFC is not substantial at  $U_F$  lower than 0.85.
4. The analysis of the effect that fuel inlet temperature has on the exergy efficiency of both the SOFC and the SOFC-VARS system demonstrates a bending-over behavior that becomes more pronounced at higher  $U_F$  values. The significance of this behavior results from the irreversibilities caused by other mechanisms such as the electronic and ionic conduction in the SOFC.
5. The exergy efficiency of both the SOFC and SOFC-VARS system is slightly sensitive to steam-to-carbon ratio, notwithstanding the temperature.
6. The effect of steam-to-carbon ratio on exergy efficiency at different values of  $U_F$  is noticeably more pronounced at higher  $U_F$ . This suggests that a more detailed analysis has to be carried out to unveil the root causes.

7. The components where most of the input exergy is destroyed are the heat exchangers, the SOFC, the afterburner and the generator. This is an advantage of the exergy analysis since it permits to pinpoint the main components where useful energy is destroyed. So efforts to improve the total system efficiency have to be targeted at these components.

Finally, it only remains to say it would be interesting to know if this model is economical and environmentally attractive and it is a project underway.

## Author details

Victor Hugo Rangel-Hernández\*, Andrés M. Niño-Avendaño, José J. Ramírez-Minguela, Juan M. Belman-Flores and Francisco Elizalde-Blancas

\*Address all correspondence to: vrangel@ugto.mx

Mechanical Engineering Department, Engineering Division, University of Guanajuato, México

## References

- [1] Huang K, Goodenough JB. Solid oxide fuel cell technology: Principles, performance and operations. 1st ed. Boca Raton, FL: North America CRC Press LLC; 2009. 340 p. ISBN: 978-1-84569-628-3
- [2] Ramadhani F, Hussain MA, Mokhlis H, Hajimolana S. Optimization strategies for solid oxide fuel cell (SOFC) application: A literature survey. *Renew Sustain Energy Rev.* 2017; **76**:460-484. DOI: 10.1016/j.rser.2017.03.052
- [3] Balki MK, Sayin C. The effect of compression ratio on the performance, emissions and combustion of an SI (spark ignition) engine fueled with ethanol, methanol and unleaded gasoline. *Energy.* 2014;**71**:194-201. DOI: 10.1016/j.energy.2014.04.074
- [4] Sghaier SF, Khin T, Brahim AB. Energetic and exergetic parametric study of a SOFC-GT hybrid power plant. *International Journal of Hydrogen Energy.* 2017;**43**:3542-3554. DOI: 10.1016/j.ijhydene.2017.08.216
- [5] Akkaya AV, Sahin B, Huseyin Erdem H. An analysis of SOFC/GT CHP system based on exergetic performance criteria. *International Journal of Hydrogen Energy.* 2008;**33**:2566-2577. DOI: 10.1016/j.ijhydene.2008.03.013
- [6] Ghanbari BP. Energy and exergy analysis of internal reforming solid oxide fuel cell-gas turbine hybrid system. *International Journal of Hydrogen Energy.* 2007;**32**:4591-4599. DOI: 10.1016/j.ijhydene.2007.08.004
- [7] Calise F, Dentice d'Accadia M, Palombo A, Vanoli L. Simulation and exergy analysis of a hybrid solid oxide fuel cell (SOFC)-gas turbine system. *Energy.* 2006;**31**:3278-3299. DOI: 10.1016/j.energy.2006.03.006

- [8] Ranjbar F, Chitsaz A, Mahmoudi SMS, Khalilarya S, Rosen MA. Energy and exergy assessments of a novel trigeneration system based on a solid oxide fuel cell. *Energy Convers Manag.* 2014;**37**:318-327. DOI: 10.1016/j.enconman.2014.07.014
- [9] Al-Sulaiman FA, Dincer I, Hamdullahpur F. Exergy analysis of an integrated solid oxide fuel cell and organic rankine cycle for cooling, heating and power production. *Journal of Power Sources.* 2010;**195**(8):2346-2354
- [10] Arsalis A. Thermo-economic modeling and parametric study hybrid solid oxide fuel cell-gas turbine-steam turbine power plants ranging from 1.5 MWe to 10 MWe. Blacksburg, Virginia: Virginia Polytechnic Institute and State University; 2007
- [11] Ugartemendia J, Ostolaza J, Zubia I. Operating point optimization of a hydrogen fueled hybrid solid oxide fuel cell-steam turbine (SOFC-ST) plant. *Energies.* 2013;**6**:5046-5068
- [12] Panopoulos KD, Fryda L, Karl J, Poulou S, Kakaras E. High temperature solid oxide fuel cell integrated with novel allothermal biomass gasification. Part II: Exergy analysis. *Journal of Power Sources.* 2006;**159**:586-594. DOI: 10.1016/j.jpowsour.2005.11.040
- [13] Gholamian E, Zare V. A comparative thermodynamic investigation with environmental analysis of SOFC waste to power conversion employing Kalina and Organic Rankine Cycles. *Energy Conversion and Management.* 2016;**117**:150-156. DOI: 10.1016/j.enconman.2016.03.011
- [14] Siddiqui O, Dincer I. Analysis and performance assessment of a new solar-based multigeneration system integrated with ammonia fuel cell and solid oxide fuel cell-gas turbine cycle. *Journal of Power Sources.* 2017;**370**:138-154. DOI: 10.1016/j.jpowsour.2017.10.008
- [15] Chitsaz A, Hosseinpour J, Assadi M. Effect of recycling on the thermodynamic and thermo-economic performances of SOFC based on trigeneration systems: A comparative study. *Energy.* 2017;**124**:613-624. DOI: 10.1016/j.energy.2017.02.019
- [16] Mehrpuoya M, Sayyad S, Zonouz MJ. Energy, exergy and sensitivity analysis of a hybrid combined cooling, heating and power (CCHP) plant with molten carbonate fuel cell (MCFC) and stirling engine. *Journal of Cleaner Production.* 2017;**148**:283-294. DOI: 10.1016/j.jclepro.2017.01.157
- [17] Chang H, Wan Z, Zheng Y, Chen X, Shu S, Tu Z, Chan SH, Cheng R, Wang X. Energy and exergy-based working fluid selection and performance analysis of a high-temperature PEMFC-based micro combined cooling heating and power system. *Applied Energy.* 2017;**204**:446-458. DOI: 10.1016/j.apenergy.2017.07.031
- [18] Balki MK, Sayin C, Canakci M. The effect of different alcohol fuels on the performance, emissions and combustion characteristics of a gasoline engine. *Fuel.* 2014;**115**:901-906
- [19] Tippawan P, Arpornwichanop A, Dincer I. Energy and exergy analysis of an ethanol-fueled solid oxide fuel cell for a trigeneration system. *Energy.* 2015;**87**:228-239. DOI: 10.1016/j.energy.2015.04.072

- [20] Hosseinpour J, Sadeghi M, Chitsaz A, Ranjbar F, Rosen MA. Exergy assessment and optimization of a cogeneration system based on a solid oxide fuel cell integrated with a Stirling engine. *Energy Convers Manag.* 2017;**143**:448-458. DOI: 10.1016/j.enconman.2017.04.021
- [21] Shamoushaki M, Ehyaei MA, Ghanatir F. Exergy, economic and environmental analysis and multi-objective optimization of a SOFC-GT power plant. *Energy.* 2017;**134**:515-531. DOI: 10.1016/j.energy.2017.06.058
- [22] Tao G, Armstrong T, Virkar A. Intermediate temperature solid oxide fuel cell (IT-SOFC) research and development activities at MSRI. In: Nineteenth Annual ACERC & ICES Conference, Utah, USA
- [23] Herold KE, Radermacher R, Klein SA. Adsorption chillers and heat pumps. 2nd ed. Boca Raton, FL: North America CRC Press LLC; 1996. 354 p. ISBN: 978-14987-1435-8
- [24] Singhal SC, Kendall K. High temperature solid oxide fuel cells: Fundamentals, design and applications. 1st ed. Oxford: Elsevier Limited; 2003. 406 p. ISBN: 9780080508085
- [25] El-Emam RS, Dincer I, Naterer GF. Energy and exergy analysis of an integrated SOFC and coal gasification system. *International Journal of Hydrogen Energy.* 2012;**37**:1689-1697. DOI: 10.1016/j.ijhydene.2011.09.139
- [26] Chan SH, Ho HK, Tian Y. Modelling of simple hybrid solid oxide fuel cell and gas turbine power plant. *Journal of Power Sources.* 2002;**109**:111-120
- [27] Larminie J, Dicks A. Fuel cell system explained. 2nd ed. Wiley; 2003, 428 p. ISBN: 978-0-470-84857-9
- [28] Kotas TJ. The exergy method of thermal power plants. Malabar Fl: Krieger Publishing Co.; 1995. ISBN: 978-0-408-01350-5
- [29] Szargut J, Morris DR, Steward FR. Exergy analysis of thermal, chemical and metallurgical processes. 1st ed. Taylor & Francis Inc.; 1988. 332 p. ISBN: 978-0-891-16574-3
- [30] Palacios-Bereche R, Gonzales R, Nebra SA. Exergy calculation of lithium bromide-water solution and its application in the exergetic evaluation of Adsorption refrigeration systems LiBr-H<sub>2</sub>O. *International Journal of Energy Research.* 2012;**36**:166-181
- [31] Kim DS, Infante Ferreira CA. A Gibbs energy equation for LiBr aqueous solutions. *International Journal of Refrigeration.* 2006;**29**:36-46
- [32] Khaliq A. Exergy analysis of gas turbine trigeneration system for combined production of power heat and refrigeration. *International Journal of Refrigeration.* 2009;**32**:534-545. DOI: 10.1016/j.ijrefrig.2008.06.007